Enhancing the Weak Signal With Arbitrary High-Frequency by Vibrational Resonance in Fractional-Order Duffing Oscillators

J. H. Yang[1]
School of Mechatronic Engineering,
China University of Mining and Technology,
Xuzhou 221116, China;
Department of Mechanical Engineering,
University of Michigan,
Ann Arbor, MI 48109;
Jiangsu Key Laboratory of Mine Mechanical and
Electrical Equipment,
China University of Mining and Technology,
Xuzhou 221116, China
e-mail: jianhuayang@cumt.edu.cn

Miguel A. F. Sanjuán
Nonlinear Dynamics,
Chaos and Complex Systems Group,
Departamento de Física,
Universidad Rey Juan Carlos,
Tulipán s/n,
Móstoles 28933, Madrid, Spain;
Institute for Physical Science and Technology,
University of Maryland,
College Park, MA 20742

H. G. Liu
School of Mechatronic Engineering,
China University of Mining and Technology,
Xuzhou 221116, China

When the traditional vibrational resonance (VR) occurs in a nonlinear system, a weak character signal is enhanced by an appropriate high-frequency auxiliary signal. Here, for the harmonic character signal case, the frequency of the character signal is usually smaller than 1 rad/s. The frequency of the auxiliary signal is dozens of times of the frequency of the character signal. Moreover, in the real world, the characteristic information is usually indicated by a weak signal with a frequency in the range from several to thousands rad/s. For this case, the weak high-frequency signal cannot be enhanced by the traditional mechanism of VR, and as such, the application of VR in the engineering field could be restricted. In this work, by introducing a scale transformation, we transform high-frequency excitations in the original system to low-frequency excitations in a rescaled system. Then, we make VR to occur at the low frequency in the rescaled system, as usual. Meanwhile, the VR also occurs at the frequency of the character signal in the original system. As a result, the weak character signal with arbitrary high-frequency can be enhanced. To make the rescaled system in a general form, the VR is investigated in fractional-order Duffing oscillators. The form of the potential function, the fractional order, and the reduction scale are important factors for the strength of VR.
[DOI: 10.1115/1.4036479]

Keywords: vibrational resonance, weak high-frequency signal, fractional-order oscillator, rescaling transformation

1 Introduction

There are many ways to improve a weak signal. Among them, the stochastic resonance (SR) method is extraordinary. In the SR theoretical framework, a proper amount of noise has a positive role on the signal detection. In the last 30 years, many references have been published on this topic [1]. A typical SR model contains three basic ingredients, i.e., a nonlinear system, a weak input signal, and an amount of noise. Usually, the weak low-frequency signal is considered as the coherent input. The signal-to-noise ratio of the output depends on the frequency of the input. For the low-frequency case, the signal-to-noise ratio will be improved by the noise. If the frequency of the input signal is a little higher, the SR phenomenon vanishes and the weak signal cannot be enhanced in this case. Hence, the frequency of the weak signal is far lower than 1 rad/s in the former investigations on SR. Moreover, the noise in the excitations is a weak noise. Otherwise the SR phenomenon will disappear. However, in many practical situations, the weak character signal which indicates the information is a high-frequency signal. For example, a signal indicating a mechanical fault usually lies in the scope of several to thousands Hz [2]. Furthermore, the weak character information is surged into the strong noise background. This kind of information cannot be detected through the traditional SR theoretical framework. To solve the problem, some techniques such as the frequency-shifted and the rescaling method are used [3].

Another phenomenon similar to the SR is the VR [4]. The VR studies a nonlinear system that is excited by a weak character signal and the other auxiliary high-frequency signal. If the weak character signal is a low-frequency harmonic signal, the response amplitude of the output at the low-frequency versus the amplitude or the frequency of the auxiliary signal presents an inverted bell configuration [4,5]. If the weak character signal is an aperiodic signal, the correlation coefficient of the output to the character signal versus the amplitude of the auxiliary signal shows a resonance-like pattern [6]. Specifically, by adjusting the auxiliary high-frequency signal, the weak character signal can be enhanced excellently. Up to present, the VR has been investigated in many kinds of systems [7–15]. However, to our knowledge, most of works on VR are focused on improving the weak low-frequency character signal. As a matter of fact, the frequency of the weak character signal is very low, usually smaller than 1 rad/s. To our knowledge, there are no references where the objective has been to enhance the weak high-frequency signal by the VR method. As we mentioned above, the weak character information is usually in a high-frequency signal form in the engineering field. The traditional VR cannot deal with this technical problem due to the fact that the response will be very small when the system is excited by high-frequency signals. Further, compared with the SR, the VR is much easier for control. Hence, it is important to propose a method to enhance the weak high-frequency signal by a new VR method. This is the main motivation of this paper.

Compared with the ordinary differential system, the fractional-order system has advantages on the response of a system. For example, via tuning the fractional order, the VR can be optimized [16–18], and the stability of the system can be enhanced [19]. The ordinary differential equation can be treated as a special case of the fractional-order system. By virtue of this reason, we

---

investigate the VR at an arbitrary high frequency in a fractional-order Duffing oscillator. The outline of the paper is organized as follows: In Sec. 2, by introducing a scale transformation, the theoretical formulation of VR in the original and rescaled systems is given. The overdamped fractional-order system and the underdamped fractional-order system are considered, respectively. In Sec. 3, the numerical simulations are carried out to verify the theoretical predictions. The detailed analysis is given in this section. In Sec. 4, some potential applications of the results are discussed. In Sec. 5, we describe briefly the main results of this paper.

2 Theoretical Formulation

In this section, we will give the theoretical analysis for VR at an arbitrary high-frequency in the fractional-order Duffing oscillator.

2.1 Overdamped Fractional-Order Duffing Oscillator.
First, we consider a fractional-order Duffing oscillator in an overdamped version. The governing equation is in a general from, i.e.,

$$\frac{d^\alpha x(t)}{dt^\alpha} + ax(t) + bx^3(t) = f\cos(\omega t) + F\cos(\Omega t) \quad (1)$$

There are several kinds of definitions for the fractional-order derivative, such as the Caputo definition, the Riemann–Liouville definition, and the Grünwald–Letnikov definition [20]. The Grünwald–Letnikov definition is described in the form

$$\left.\frac{d^\alpha x(t)}{dt^\alpha}\right|_{t=kh} = \lim_{h\to 0}\frac{1}{h^\alpha}\sum_{j=0}^{k}(-1)^j\binom{\alpha}{j}x(kh - jh) \quad (2)$$

The binomial coefficient $\binom{\alpha}{j}$ is given by

$$\binom{\alpha}{j} = \frac{\alpha!}{j!(\alpha - j)!} = \frac{\Gamma(\alpha+1)}{\Gamma(j+1)\Gamma(\alpha - j + 1)} \quad (3)$$

where $\Gamma(\bullet)$ is the gamma function. In Eq. (1), $f\cos(\omega t)$ is a weak high-frequency signal and we call it as character signal for simplicity. It is different from all cases in the previous works [16–18,21–29], even though, the frequency of the weak signal is usually low. However, in the engineering background, the characteristic information is a weak high-frequency signal. For example, in our former study, the vibration characteristic of a fault planetary gear is a signal with the magnitude of the order of 10^{-3} m/s^2 and the frequency of the order of 10^2 Hz [2]. In this work, some different values of the high-frequency ω on the response will be discussed. Another harmonic signal $F\cos(\Omega t)$ is an auxiliary signal. The frequencies of the two signals satisfy $\Omega \gg \omega$. Considering the engineering background, the value of the fractional order usually lies in the interval (0, 2). The coefficients a and b have different physical meaning for different model. For example, for a mechanical mode, they may represent the stiffness of the linear spring and the nonlinear spring, respectively. Here, we only consider the fractional-order system as a signal processor. It can be realized by the circuit device. The potential function of Eq. (1) is $V(x) = (a/2)x^2 + (b/4)x^4$. If $a < 0$ and $b > 0$, the potential function is in the double-well form. Otherwise, if $a > 0$ and $b > 0$, the potential function is in the single-well form.

The excitations in Eq. (1) are both high-frequency excitations. According to the frequency response characteristic of the vibration theory, the response amplitude is very small [30]. Hence, we need to shift the high frequency to the low frequency through a rescaling transformation. First, let $\tau = \beta t$ and $x(t) = z(\tau)$. The parameter β is the time scale for reduction. Then, according to the Grünwald–Letnikov definition in Eq. (2) and the scale change theorem of the fractional-order derivative [31], we have

$$\left.\frac{d^\alpha x(t)}{dt^\alpha}\right|_{t=kh} = \beta^\alpha\lim_{h\to 0}\frac{1}{(\beta h)^\alpha}\sum_{j=0}^{k}(-1)^j\binom{\alpha}{j}x[\beta(kh - jh)]$$
$$= \beta^\alpha\left.\frac{d^\alpha x(\tau)}{d\tau^\alpha}\right|_{\tau=\beta t} \quad (4)$$

Further, we obtain the equation in the time scale τ

$$\frac{d^\alpha z(\tau)}{d\tau^\alpha} + \frac{a}{\beta^\alpha}z(\tau) + \frac{b}{\beta^\alpha}z^3(\tau) = \frac{f}{\beta^\alpha}\cos\left(\omega\frac{\tau}{\beta}\right) + \frac{F}{\beta^\alpha}\cos\left(\Omega\frac{\tau}{\beta}\right) \quad (5)$$

Equation (5) has the same dynamical property as Eq. (1). If the values of the coefficients a/β^α and b/β^α in Eq. (5) have the same order with the coefficients a and b in Eq. (1), the response of Eq. (5) will also have the same magnitude with Eq. (1). Another thing, we must note that the magnitudes of the high-frequency signals have been decreased to $1/\beta^\alpha$ compared with the original excitations. Hence, we need to recover them to the original in the rescaled system. Hence, Eq. (5) is rewritten to

$$\frac{d^\alpha z(\tau)}{d\tau^\alpha} + \frac{a}{\beta^\alpha}z(\tau) + \frac{b}{\beta^\alpha}z^3(\tau) = f\cos\left(\omega\frac{\tau}{\beta}\right) + F\cos\left(\Omega\frac{\tau}{\beta}\right) \quad (6)$$

Let $a_1 = (a/\beta^\alpha)$, $b_1 = (b/\beta^\alpha)$, $\omega_1 = (\omega/\beta)$, $\Omega_1 = (\Omega/\beta)$, then Eq. (6) turns to

$$\frac{d^\alpha z(\tau)}{d\tau^\alpha} + a_1 z(\tau) + b_1 z^3(\tau) = f\cos(\omega_1\tau) + F\cos(\Omega_1\tau) \quad (7)$$

Equation (7) has the same dynamical property as Eq. (1). From our former research [16], we know that the VR will occur in Eq. (7). As a result, the weak high-frequency character signal will be detected in the rescaled system. From Eqs. (5)–(7), the system is rescaled. When the VR occurs in the rescaled system, it also occurs in the original system simultaneously. This method has been successfully applied in the investigation of the SR induced by the weak high-frequency character signal [32–35].

The solution of Eq. (7) can be solved by some approximate methods, such as the multiscale method, the averaging method, and the perturbation method. Among them, the method of direct partition of motions is widely used in lots of models for its simplicity in engineering fields, although it is sensitive to the excitations [16–18,21–25]. In the engineering fields, this method can satisfy the requirement. Hence, the method of direct partition of motions is used in the theoretical analysis in the following manner. According to this method, let $z = Z + \Psi$, where Z and Ψ are the slow variable and the fast variable with period $2\pi/\omega$ and $2\pi/\Omega$, respectively, then we have

$$\frac{d^\alpha Z}{d\tau^\alpha} + \frac{d^\alpha\Psi}{d\tau^\alpha} + a_1 Z + a_1\Psi + b_1 Z^3 + 3b_1 Z^2\Psi + 3b_1 Z\Psi^2 + b_1\Psi^3$$
$$= f\cos(\omega_1\tau) + F\cos(\Omega_1\tau) \quad (8)$$

Seeking an approximate solution of the fast variable Ψ in the linear equation

$$\frac{d^\alpha\Psi}{d\tau^\alpha} + a_1\Psi = F\cos(\Omega_1\tau) \quad (9)$$

Letting

$$\Psi = \frac{F}{\mu}\cos(\Omega_1\tau - \theta) \quad (10)$$

then we have

$$\frac{d^\alpha\Psi}{d\tau^\alpha} = \frac{F}{\mu}\Omega^\alpha\cos\left(\Omega_1\tau - \theta + \frac{\alpha\pi}{2}\right)$$
$$= \frac{F}{\mu}\Omega^\alpha\left[\cos\frac{\alpha\pi}{2}\cos(\Omega_1\tau - \theta) - \sin\frac{\alpha\pi}{2}\sin(\Omega_1\tau - \theta)\right] \quad (11)$$

at the same time

$$
\begin{aligned}
F \cos (\Omega_1 \tau) &= F \cos (\Omega_1 \tau - \theta + \theta) \\
&= F \cos \theta \cos(\Omega_1 \tau - \theta) - F \sin \theta \sin(\Omega_1 \tau - \theta) \quad (12)
\end{aligned}
$$

substituting Eqs. (11) and (12) into Eq. (9), by using the undetermined coefficient method, i.e., comparing the coefficients of the terms $\cos(\Omega_1 \tau - \theta)$ and $\sin(\Omega_1 \tau - \theta)$, we get equation groups

$$
\begin{cases}
a_1 + \Omega^\alpha \cos \dfrac{\alpha\pi}{2} = \mu \cos \theta \\[2mm]
\Omega^\alpha \sin \dfrac{\alpha\pi}{2} = \mu \sin \theta
\end{cases}
\quad (13)
$$

Solving the equation groups above, we obtain

$$
\mu^2 = \left(a_1 + \Omega_1^\alpha \cos \frac{\alpha\pi}{2} \right)^2 + \left(\Omega_1^\alpha \sin \frac{\alpha\pi}{2} \right)^2 \quad (14)
$$

and

$$
\theta = \tan^{-1} \frac{\Omega_1^\alpha \sin \dfrac{\alpha\pi}{2}}{a_1 + \Omega_1^\alpha \cos \dfrac{\alpha\pi}{2}} \quad (15)
$$

Substituting Eq. (10) into Eq. (8) and averaging all terms over the interval $[0, 2\pi/\Omega_1]$, we obtain

$$
\frac{d^\alpha Z}{d\tau^\alpha} + \gamma Z + b_1 Z^3 = f \cos(\omega_1 \tau) \quad (16)
$$

where

$$
\gamma = a_1 + \frac{3b_1 F^2}{2\mu^2} \quad (17)
$$

If $f = 0$, the equilibria of the equivalent system (16) are

$$
Z_o^* = 0, \quad Z_\pm^* = \pm \sqrt{-\frac{\gamma}{b_1}} \quad (18)
$$

If $\gamma < 0$, Eq. (16) has two stable equilibria $Z_\pm^* = \pm\sqrt{-(\gamma/b_1)}$ and one unstable equilibrium $Z_o^* = 0$. Otherwise, if $\gamma \geq 0$, Eq. (16) only has one stable $Z_o^* = 0$. Thus, the equilibria of Eq. (16) depend on the sign of the parameter γ. Further, in Eq. (17), the sign of γ is mainly determined by the system coefficients a, b, the auxiliary signal amplitude F, the auxiliary signal frequency Ω, the fractional-order α, and the reduction scale β.

To get the solution of the slow motion at the frequency ω_1, we eliminate the constant component in the response. Let $y = Z - Z^*$, where Z^* is the stable equilibrium defined in Eq. (18), then we have

$$
\frac{d^\alpha Y}{d\tau^\alpha} + \omega_r^2 Y + 3b_1 Z^* Y + b_1 Y^3 = f \cos(\omega_1 \tau) \quad (19)
$$

where $\omega_r^2 = \gamma + 3b_1 Z^{*2}$. The approximate response at the frequency ω_1 is solved by the linear equation

$$
\frac{d^\alpha Y}{dt^\alpha} + \omega_r^2 Y = f \cos(\omega_1 \tau) \quad (20)
$$

When $t \to +\infty$, the solution of Eq. (20) is

$$
Y = A_L \cos(\omega_1 \tau - \varphi) \quad (21)
$$

where

$$
A_L = \frac{f}{\sqrt{\left(\omega_r^2 + \omega_1^\alpha \cos \dfrac{\alpha\pi}{2} \right)^2 + \left(\omega_1^\alpha \sin \dfrac{\alpha\pi}{2} \right)^2}} \quad (22)
$$

$$
\varphi = \tan^{-1} \frac{\omega_1^\alpha \sin \dfrac{\alpha\pi}{2}}{\omega_r^2 + \omega_1^\alpha \cos \dfrac{\alpha\pi}{2}} \quad (23)
$$

To quantify the performance of a system to enhance the weak signal, a quantitative index named response amplitude is usually used which is defined by

$$
Q = \frac{A_L}{f} = \frac{1}{\sqrt{\left(\omega_r^2 + \omega_1^\alpha \cos \dfrac{\alpha\pi}{2} \right)^2 + \left(\omega_1^\alpha \sin \dfrac{\alpha\pi}{2} \right)^2}} \quad (24)
$$

Through analysis of the response amplitude Q in Eq. (24), the enhancement of the weak high-frequency signal by the overdamped fractional-order Duffing oscillator can be discussed.

2.2 Underdamped Fractional-Order Duffing Oscillator. Now, we consider the underdamped fractional-order Duffing oscillator

$$
\frac{d^2 x}{dt^2} + \delta \frac{d^\alpha x(t)}{dt^\alpha} + ax(t) + bx^3(t) = f \cos(\omega t) + F \cos(\Omega t) \quad (25)
$$

The parameter δ is the coefficient of the fractional-order damping. Other parameters in Eq. (25) are the same as the ones appearing in Eq. (1). Through the scale transformation $\tau = \beta t$ and $x(t) = z(\tau)$, we obtain

$$
\frac{d^2 z(\tau)}{d\tau^2} + \frac{\delta\beta^\alpha}{\beta^2} \frac{d^\alpha z(\tau)}{dt^\alpha} + \frac{a}{\beta^2} z(\tau) + \frac{b}{\beta^2} z^3(\tau) = \frac{f}{\beta^2} \cos(\omega\tau) + \frac{F}{\beta^2} \cos(\Omega\tau) \quad (26)
$$

We need to recover the damped force and the excitations to the original magnitude. Thus

$$
\frac{d^2 z(\tau)}{d\tau^2} + \delta \frac{d^\alpha z(\tau)}{dt^\alpha} + a_1 z(\tau) + b_1 z^3(\tau) = f \cos(\omega\tau) + F \cos(\Omega\tau) \quad (27)
$$

where $a_1 = a/\beta^2$ and $b_1 = b/\beta^2$. Let $z = Z + \Psi$, then we obtain

$$
\begin{aligned}
\frac{d^2 Z}{d\tau^2} + \frac{d^2 \Psi}{d\tau^2} + \delta \frac{d^\alpha Z}{d\tau^\alpha} + \delta \frac{d^\alpha \Psi}{d\tau^\alpha} + a_1 Z + a_1 \Psi + b_1 Z^3 + 3b_1 Z^2 \Psi \\
+ 3b_1 Z\Psi^2 + b_1 \Psi^3 = f \cos(\omega_1 \tau) + F \cos(\Omega_1 \tau) \quad (28)
\end{aligned}
$$

Searching for the approximate solution of Ψ in the linear equation

$$
\frac{d^2 \Psi}{d\tau^2} + \delta \frac{d^\alpha \Psi}{d\tau^\alpha} + a_1 \Psi = F \cos(\Omega_1 \tau) \quad (29)
$$

we obtain

$$
\Psi = \frac{F}{\mu} \cos(\Omega_1 \tau - \theta) \quad (30)
$$

where

$$
\mu^2 = \left(a_1 + \delta\Omega_1^\alpha \cos \frac{\alpha\pi}{2} - \Omega_1^2 \right)^2 + \left(\delta\Omega_1^\alpha \sin \frac{\alpha\pi}{2} \right)^2 \quad (31)
$$

and

$$
\theta = \tan^{-1} \frac{\delta\Omega_1^\alpha \sin \dfrac{\alpha\pi}{2}}{a_1 + \delta\Omega_1^\alpha \cos \dfrac{\alpha\pi}{2} - \Omega_1^2} \quad (32)
$$

Substituting Eq. (30) into Eq. (28) and averaging all terms over the interval $[0, 2\pi/\Omega_1]$, one has

$$\frac{d^2Z}{d\tau^2} + \delta\frac{dZ}{d\tau} + \gamma Z + b_1 Z^3 = f\cos(\omega_1\tau) \quad (33)$$

where $\gamma = a_1 + ((3b_1 F^2)/2\mu^2)$. The equilibria X^* are still given in Eq. (18). To eliminate the constant in Eq. (33), we let $Y = Z - Z^*$. Then, we obtain

$$\frac{d^2Y}{d\tau^2} + \delta\frac{d^\alpha Y}{d\tau^\alpha} + \omega_r^2 Y + 3b_1 Z^* Y^2 + b_1 Y^3 = f\cos(\omega_1\tau) \quad (34)$$

where $\omega_r^2 = \gamma + 3b_1 Z^{*2}$. Searching the solution of Y in the linear equation

$$\frac{d^2Y}{d\tau^2} + \delta\frac{d^\alpha Y}{d\tau^\alpha} + \omega_r^2 Y = f\cos(\omega_1\tau) \quad (35)$$

then we obtain $Y = A_L \cos(\omega_1\tau - \varphi)$, where

$$A_L = \frac{f}{\sqrt{\left[\omega_r^2 - \left(\omega_1^2 - \delta\omega_1^\alpha \cos\frac{\alpha\pi}{2}\right)\right]^2 + \left(\delta\omega_1^\alpha \sin\frac{\alpha\pi}{2}\right)^2}} \quad (36)$$

and

$$\varphi = \tan^{-1}\frac{\delta\omega_1^\alpha \sin\frac{\alpha\pi}{2}}{\omega_r^2 - \left(\omega_1^2 - \delta\omega_1^\alpha \cos\frac{\alpha\pi}{2}\right)} \quad (37)$$

Hence, the response amplitude of the underdamped fractional-order oscillator is

$$Q = \frac{1}{\sqrt{\left[\omega_r^2 - \left(\omega_1^2 - \delta\omega_1^\alpha \cos\frac{\alpha\pi}{2}\right)\right]^2 + \left(\delta\omega_1^\alpha \sin\frac{\alpha\pi}{2}\right)^2}} \quad (38)$$

3 Numerical Simulations

We use numerical simulations to verify the analytical results. For the numerical simulation, the response amplitude at the frequency ω is computed by

$$Q = \frac{\sqrt{B_s^2 + B_c^2}}{f} \quad (39)$$

where B_s and B_c are the sine and the cosine components of the Fourier coefficients

$$B_s = \frac{2}{nT}\int_0^{nT} x(t)\sin(\omega t)dt, \quad B_c = \frac{2}{nT}\int_0^{nT} x(t)\cos(\omega t)dt \quad (40)$$

In Eq. (40), $T = 2\pi/\omega$ and n is an integer number which is large enough. Further, for the numerical simulations, Eqs. (1) and (25) have turned to the form

$$\frac{d^\alpha x(t)}{dt^\alpha} + ax(t) + bx^3(t) = \beta^\alpha f\cos(\omega t) + \beta^\alpha F\cos(\Omega t) \quad (41)$$

and

$$\frac{d^2x}{dt^2} + \beta^{2-\alpha}\delta\frac{d^\alpha x(t)}{dt^\alpha} + ax(t) + bx^3(t) = \beta^2 f\cos(\omega t) + \beta^2 F\cos(\Omega t) \quad (42)$$

For the numerical discretization of the fractional-order operator, the predictor-corrector algorithm will be used [36]. In the following, we let $\Omega = \beta_1\omega$ and $\beta = \beta_2\omega$. Hence, $\omega_1 = (\omega/\beta) = (1/\beta_2)$ and $\Omega_1 = (\Omega/\beta) = (\beta_1/\beta_2)$.

If the reduction scale $\beta = 1$, then the rescaled system degenerates to the original system. For the overdamped case, the response amplitude for $\beta = 1$ is given in Fig. 1. Apparently, there is no VR phenomenon in this figure. Although there is a resonance phenomenon that is induced by the fractional order, the magnitude of the response amplitude is very small. It shows that the weak high-frequency signal cannot be enhanced in Eq. (1) directly. In the following analysis described in this section, we will discuss the VR in the rescaled system.

3.1 Overdamped Fractional-Order Duffing Oscillator. In Fig. 2, the weak high-frequency signal is enhanced by the auxiliary signal for different factional-order values. In Fig. 2(a), the three-dimensional curve of the response amplitude Q versus the fractional-order α and the auxiliary signal amplitude F is given by the analytical prediction. From this subplot, we find that both the fractional order and the auxiliary signal can induce a strong resonance and lead to the improvement of the weak high-frequency character signal. To verify the validity of the analytical results, the numerical simulations are also given in Figs. 2(b)–2(f) for different values of the fractional order. Notice that the analytical results describe the VR in the rescaled system and the numerical results describe the VR in the original system. In these subplots, the analytical results are in good agreement with the numerical simulations. It explains the equivalence of the rescaled system and the original system. It also indicates the validity of the analytical method. In this figure, with the increase of the fractional order, the magnitudes of both the resonance peak and the corresponding value of F will increase also. It illustrates that the fractional-order system can improve the weak signal especially for the case $\alpha > 1$. Hence, it is important to design a fractional-order system for enhancing a weak signal. Another thing, with the increase of the fractional order, the pattern of the curve turns from the single-peak mode to the double-peak mode. It is the same with the case in the fractional-order system excited by two low-frequency signals [16]. Hence, it is not necessary to give further explanations here.
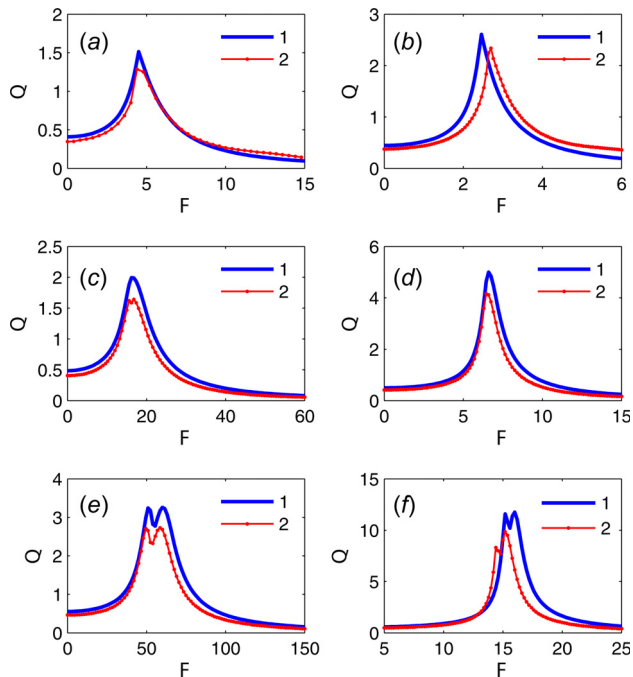
In Fig. 3, the VR phenomenon is shown for different values of β_2. Because $\omega_1 = (1/\beta_2)$, the low frequency in the rescaled system is $\omega_1 = 0.5$ in Figs. 3(a), 3(c), and 3(e) and $\omega_1 = 0.2$ in Figs. 3(b),
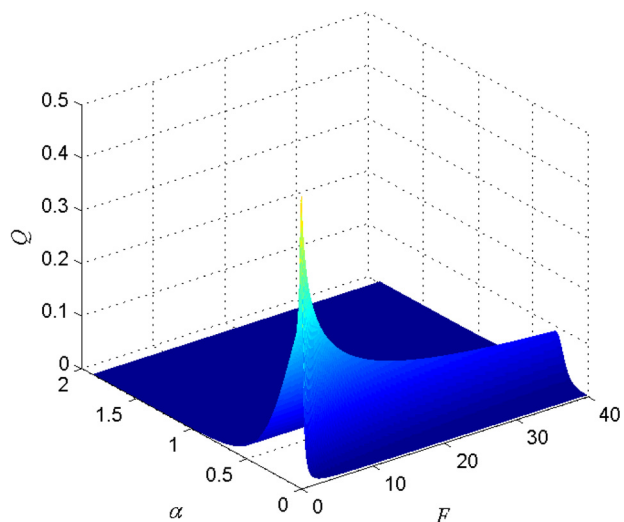
Fig. 1 The three-dimensional curve of the response amplitude Q in which there is no VR occurring at the frequency ω. The simulation parameters are $\omega = 1500$, $f = 0.01$, $\beta_1 = 40$, $\beta = 1$, $a_1 = -1$, $b_1 = 1$.
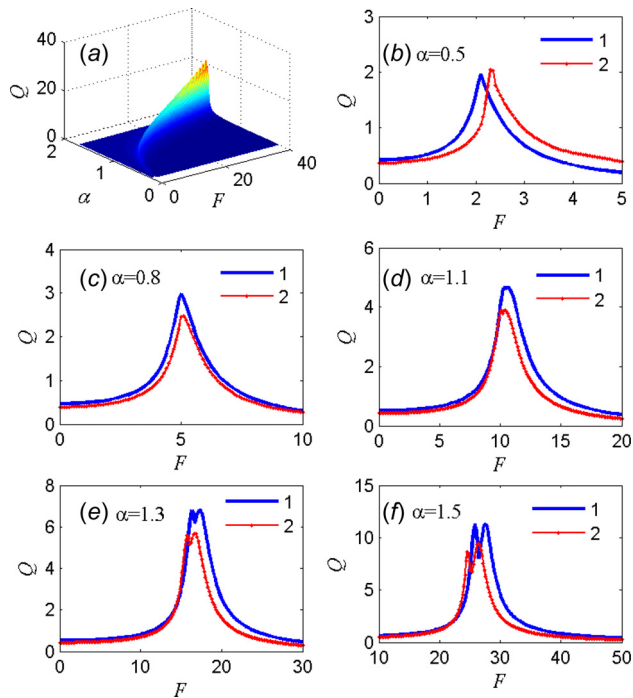
Fig. 2 The VR phenomenon occurs at the frequency ω for different fractional-order values. (*a*) The three-dimensional curve of the response amplitude Q obtained by the analytical predication. (*b*)–(*f*) The response amplitude versus the signal amplitude F for different factional-order values. The simulation parameters are $\omega = 1500$, $f = 0.01$, $\beta_1 = 40$, $\beta_2 = 4$, $a_1 = -1$, $b_1 = 1$. In (*b*)–(*f*), line 1 is the analytical curve and line 2 is the numerical curve.
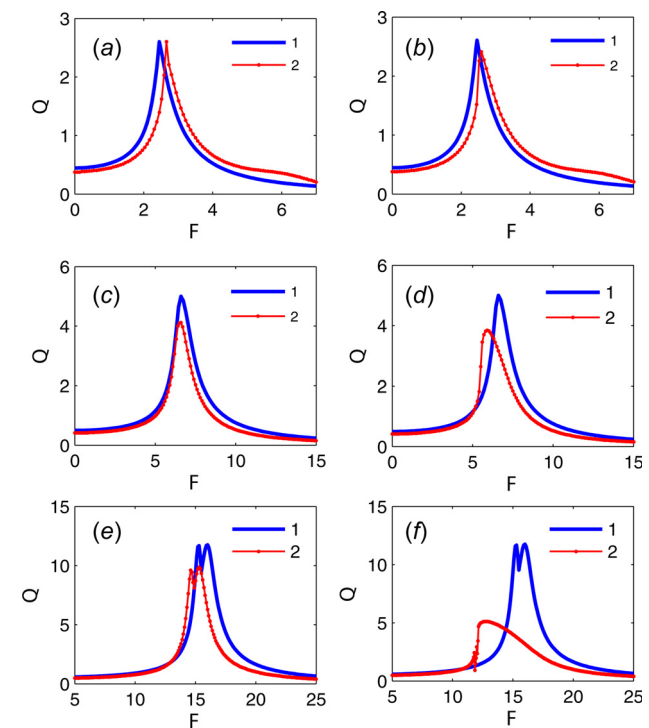
3(*d*), and 3(*f*). For lower frequency ω_1, i.e., when β_2 is larger, the response amplitude will achieve a stronger resonant state. It leads to a satisfactory effect for enhancing the weak high-frequency character signal.
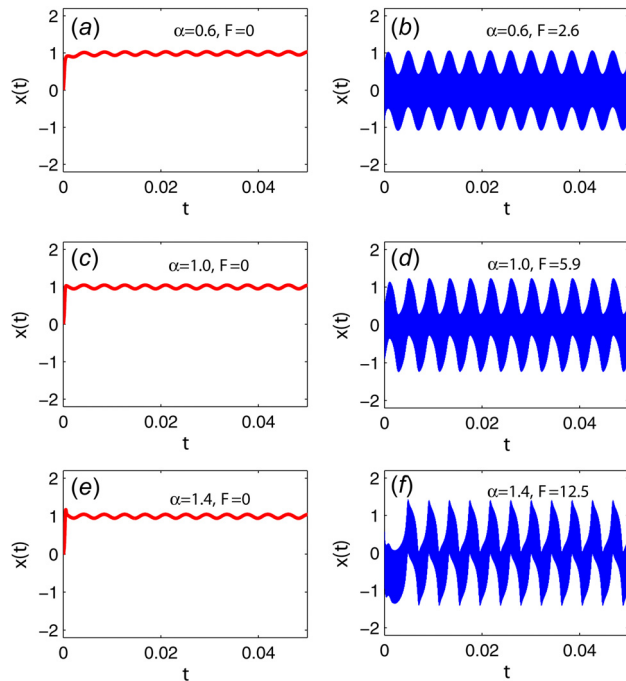
In Fig. 4, the VR is studied under different values of the amplitude of the weak high-frequency character signal. For smaller values of f and α, the numerical results and the analytical results are in good agreement as shown in Figs. 4(*a*)–4(*d*). For larger values of f and α, although the resonance occurs in both the analytical and the numerical curves, the resonance peak obtained by the numerical result may be smaller than that obtained by the analytical result. It is induced by the susceptibility of the approximate analytical method to the excitation parameters. In this problem, there are some publications to discuss it [21,22]. As we mentioned above, when other methods such as the multiscale method, the averaging method, and the perturbation method are used, the error between the analytical results and the numerical results may be smaller. We use the direct partition of motions method since it is much simpler compared with other approximate methods and it can satisfy the requirements in the engineering fields.

To understand the resonance much more clearly, the time series at the resonant state is given in Fig. 5 under different simulation parameters. When the auxiliary high-frequency signal is absent, i.e., for the case $F = 0$, the resonance disappears and the response is very weak. When we choose the simulation parameters that correspond to the resonance peak in Fig. 4, the resonance peak in the time series is apparently shown.
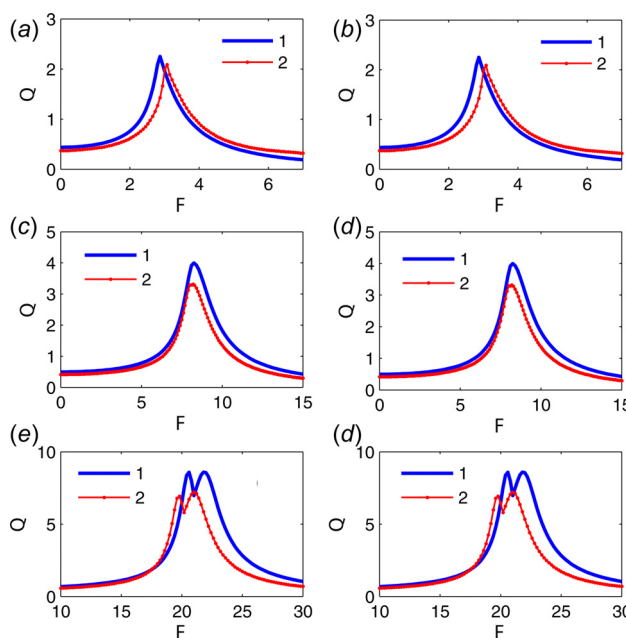
In Fig. 6, the VR phenomenon is given under different values of the fractional-order and the high-frequency ω. Because β_2 is a fixed value, the low frequency ω_1 in the rescaled system is a constant. It is independent of the signal frequency ω. As a consequence, the results for the case $\omega = 200$ and $\omega = 2000$ should be identical completely. The numerical results demonstrate this

Fig. 3 The VR phenomenon occurs at the frequency ω for different fractional-order values. The simulation parameters are $\omega = 1500$, $f = 0.01$, $\beta_1 = 40$, $a_1 = -1$, $b_1 = 1$, and in (*a*) $\alpha = 0.6$, $\beta_2 = 2$, in (*b*) $\alpha = 0.6$, $\beta_2 = 5$, in (*c*) $\alpha = 1.0$, $\beta_2 = 2$, in (*d*) $\alpha = 1.0$, $\beta_2 = 5$, in (*e*) $\alpha = 1.4$, $\beta_2 = 2$, and in (*f*) $\alpha = 1.4$, $\beta_2 = 5$. In each subplot, line 1 is the analytical curve and line 2 is the numerical curve.

Fig. 4 The VR phenomenon occurs at the frequency ω for different fractional-order values. The simulation parameters are $\omega = 1500$, $\beta_1 = 40$, $\beta_2 = 5$, $a_1 = -1$, $b_1 = 1$, and in (*a*) $\alpha = 0.6$, $f = 0.005$, in (*b*) $\alpha = 0.6$, $f = 0.1$, in (*c*) $\alpha = 1.0$, $f = 0.005$, in (*d*) $\alpha = 1.0$, $f = 0.1$, in (*e*) $\alpha = 1.4$, $f = 0.005$, and in (*f*) $\alpha = 1.4$, $f = 0.1$. In each subplot, line 1 is the analytical curve and line 2 is the numerical curve.
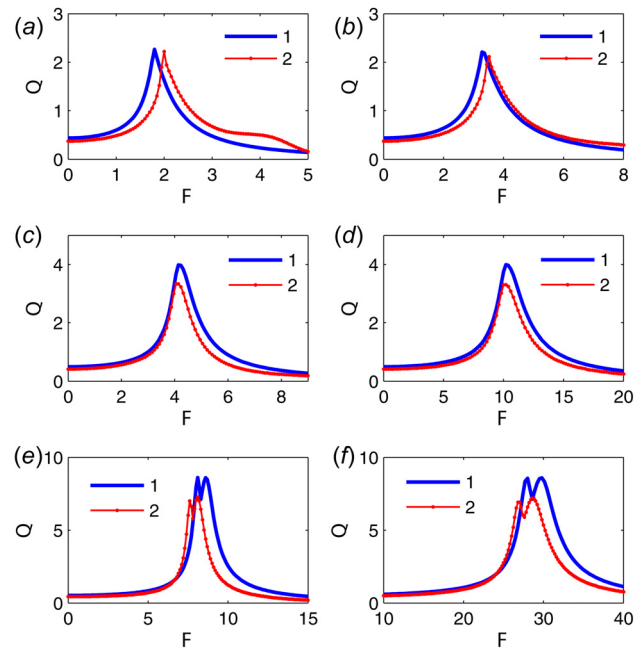
Fig. 5 The time series of the system under different fractional-order values, the simulation parameters are $f = 0.1$, $\omega = 1500$, $\beta_1 = 40$, $\beta_2 = 5$, $a_1 = -1$, $b_1 = 1$

Fig. 7 The VR phenomenon occurs at the frequency ω for different fractional-order values. The simulation parameters are $\omega = 1500$, $f = 0.1$, $\beta_2 = 4$, $a_1 = -1$, $b_1 = 1$, and in (a) $\alpha = 0.6$, $\beta_1 = 20$, in (b) $\alpha = 0.6$, $\beta_1 = 50$, in (c) $\alpha = 1.0$, $\beta_1 = 20$, in (d) $\alpha = 1.0$, $\beta_1 = 50$, in (e) $\alpha = 1.4$, $\beta_1 = 20$, and in (f) $\alpha = 1.4$, $\beta_1 = 50$. In each subplot, line 1 is the analytical curve and line 2 is the numerical curve.

is different from Figs. 7(a)–7(f). The value of β_1 influences the magnitude of F which induces the resonance. For larger value of β_1, we need larger values of F to make the resonance to occur. The value of β_1 influences the magnitude of the resonance peak slightly.
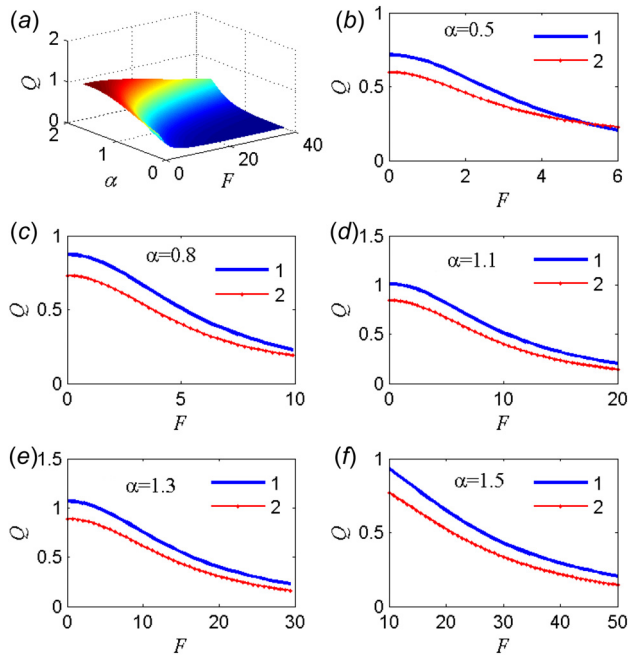
In Figs. 1–7, we choose $a_1 = -1$ and $b_1 = 1$, which indicates that the rescaled system in Eq. (7) is a typical bistable system. Moreover, from $a = a_1\beta^\alpha$ and $b = b_1\beta^\alpha$, we know that the original system is also a bistable system. In Fig. 8, we choose $a_1 = 1$ and $b_1 = 1$. Then, both the rescaled system and the original system are also monostable systems. From the analytical and numerical results, we cannot find the resonance phenomenon. No matter what value of the fractional order we choose, the response amplitude is decreased with the increase of the value of F. Hence, it is difficult to enhance the weak high-frequency character signal by the VR in monostable systems.

**3.2 Underdamped Fractional-Order Duffing Oscillator.** The underdamped oscillator is an important model for the SR and the VR [24,25,37,38]. In this subsection, we study the VR induced by the weak high-frequency character signal in the fractional-order Duffing oscillator in the underdamped version.

In Fig. 9, the three-dimensional curves of the response amplitude versus the fractional-order α and the auxiliary signal amplitude F are given by analytical results. With the increase of the coefficient of the fractional-order damping, the response amplitude will decrease. It illustrates that the fractional-order damping has the same effect as the ordinary damping. The damping consumes the energy and suppresses the response amplitude.

In Fig. 10, the VR is verified by both the analytical and the numerical results. For different values of the fractional order and the damping coefficient, the curve of the response amplitude may present the single-peak mode or the double-peak mode. Comparing Fig. 10 with Fig. 3, we find that the underdamped fractional-order system may enhance the weak high-frequency character signal in a higher level.

Fig. 6 The VR phenomenon occurs at the frequency ω for different fractional-order values. The simulation parameters are $f = 0.01$, $\beta_1 = 40$, $\beta_2 = 4$, $a_1 = -1$, $b_1 = 1$, and in (a) $\alpha = 0.6$, $\omega = 200$, in (b) $\alpha = 0.6$, $\omega = 2000$, in (c) $\alpha = 1.0$, $\omega = 200$, in (d) $\alpha = 1.0$, $\omega = 2000$, in (e) $\alpha = 1.4$, $\omega = 200$, and in (f) $\alpha = 1.4$, $\omega = 2000$. In each subplot, line 1 is the analytical curve and line 2 is the numerical curve.

prediction. Hence, the VR can occur in the nonlinear system when the weak character signal has an arbitrary high frequency.

In Fig. 7, the VR is given under different values of β_1. In other words, besides the value of the fractional-order α, the frequency Ω

Fig. 8 There is no VR phenomenon at the frequency ω in monostable systems. (*a*) The three-dimensional curve of the response amplitude Q obtained by the analytical prediction. (*b*)–(*f*) The response amplitude versus the signal amplitude F for different factional-order values. The simulation parameters are $\omega = 1500$, $f = 0.01$, $\beta_1 = 40$, $\beta_2 = 4$, $a_1 = 1$, $b_1 = 1$. In (*b*)–(*f*), line 1 is the analytical curve and line 2 is the numerical curve.

Fig. 10 The VR phenomenon occurs at the frequency ω for different fractional-order values. The simulation parameters are $f = 0.01$, $\omega = 1500$, $\beta_1 = 40$, $\beta_2 = 5$, $a_1 = -1$, $b_1 = 1$, and in (*a*) $\alpha = 0.5$, $\delta = 0.8$, in (*b*) $\alpha = 0.5$, $\delta = 1.2$, in (*c*) $\alpha = 1.0$, $\delta = 0.8$, in (*d*) $\alpha = 1.0$, $\delta = 1.2$, in (*e*) $\alpha = 1.5$, $\delta = 0.8$, and in (*f*) $\alpha = 1.5$, $\delta = 1.2$. In each subplot, line 1 is the analytical curve and line 2 is the numerical curve.
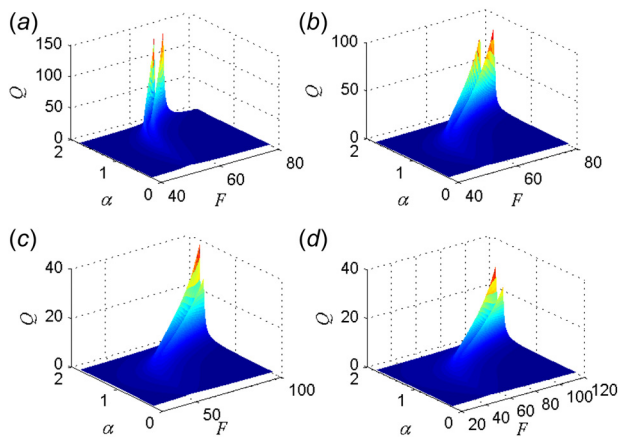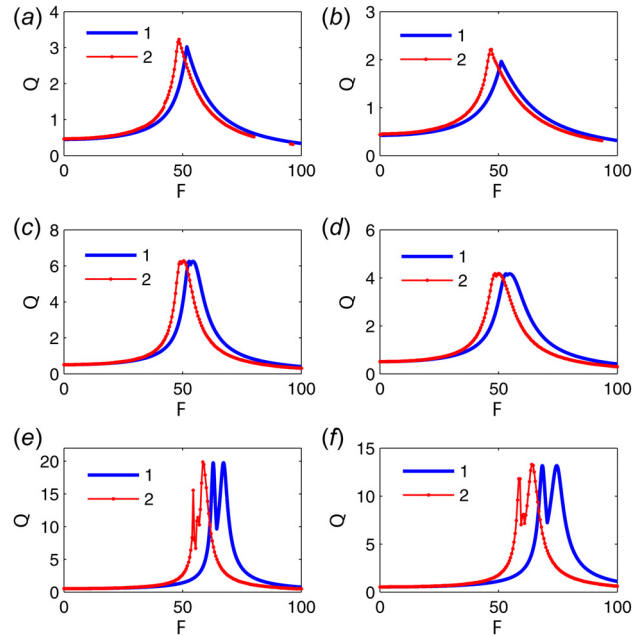

Fig. 9 The three-dimensional curve of the response amplitude Q. The simulation parameters are $f = 0.01$, $\omega = 1500$, $\beta_1 = 40$, $\beta_2 = 5$, $a_1 = -1$, $b_1 = 1$, and (*a*) $\delta = 0.4$, (*b*) $\delta = 0.7$, (*c*) $\delta = 1.5$, and (*d*) $\delta = 2$.

Fig. 11 The response amplitude versus the signal amplitude F for different factional-order values and different coefficients. The simulation parameters are $\omega = 1500$, $f = 0.01$, $\beta_1 = 40$, $\beta_2 = 5$, $a_1 = 1$, $b_1 = 1$, and (*a*) $\alpha = 0.6$, $\delta = 0.7$, (*b*) $\alpha = 0.6$, $\delta = 1.4$, (*c*) $\alpha = 1.0$, $\delta = 0.7$, (*d*) $\alpha = 1.0$, $\delta = 1.4$, (*e*) $\alpha = 1.5$, $\delta = 0.7$, and (*f*) $\alpha = 1.5$, $\delta = 1.4$. In each subplot, line 1 is the analytical curve and line 2 is the numerical curve.
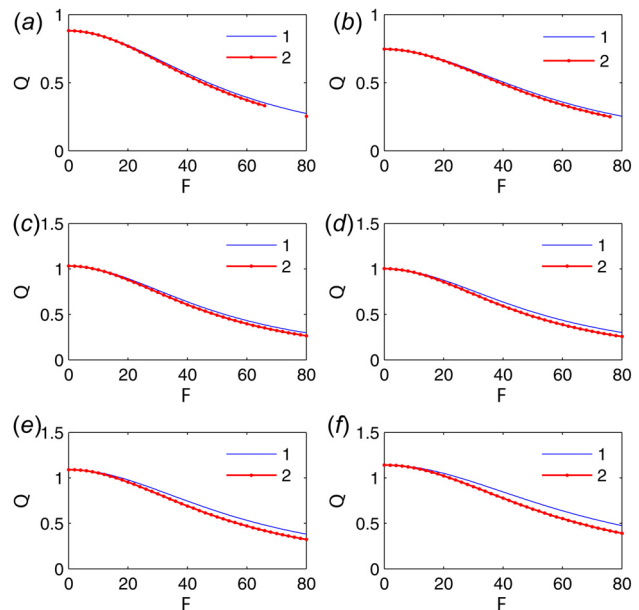
In Fig. 11, we choose $a > 0$ and $b > 0$. Then, the original system is a monostable system. In this figure, the response amplitude is a monotonic decreasing function of the auxiliary signal amplitude F. As a result, in the underdamped fractional-order system, we should choose the bistable potential but not the monostable potential to enhance the weak high-frequency character signal.

4 Some Discussions on the Potential Applications

In order to explain the idea in this work in detail, we give some discussions on the potential applications of the VR by the rescaled method.

In Fig. 12, the scheme for the VR in the bistable system by the rescaled method is illustrated clearly. When the VR is occurring, the weak character signal is enhanced. At first, we need to amplify the input. Specifically, we input the character signal and the auxiliary signal into the signal amplifier together. The amplification factor should be chosen based on the result of this paper. If we use
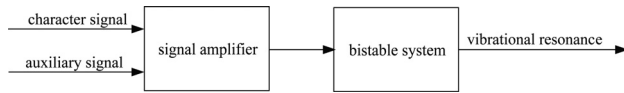
Fig. 12 The scheme for the VR at an arbitrary high frequency by the rescaled method

the system in Eq. (1) as the VR system, the amplification factor is β^α according to Eqs. (5) and (6). Moreover, if we use the system in Eq. (25) as the VR system, the amplification factor is β^2 according to Eqs. (26) and (27). The choice of β has been discussed in Sec. 5. Then, the parameters of the system are also needed to be determined by the rescaled method. If we use the system in Eq. (1) as the VR system, the system parameters are $a = a_1\beta^\alpha$ and $b = b_1\beta^\alpha$ according to Eqs. (5) and (6). Herein, a_1 and b_1 are the system parameters when the traditional VR occurs at low frequency. For example, we can choose $a_1 = -1$ and $b_1 = 1$. If we use the system in Eq. (25) as the VR system, the system parameters are $a = a_1\beta^\alpha$ and $b = b_1\beta^\alpha$ according to Eqs. (26) and (27). Moreover, we choose the fractional-order system but not the ordinary system. It is because an appropriate fractional order may enhance the weak character signal in a higher degree. The value of the fractional order, which induces the strongest resonance at the character frequency, can be determined by the optimization algorithm theoretically. Then, it can be realized with the help of the hardware. After the determination of the amplification factor and the system parameters, by adjusting the amplitude of the auxiliary signal, the VR can occur and the character signal can be enhanced. Every step cannot be ignored in the rescaled scheme. If the signals are not amplified before they input to the bistable system, the VR cannot occur and the weak character signal cannot be enhanced. Another thing, if we choose much smaller system parameters, the response will diverge and the device may be destroyed. If we choose much larger system parameters, the optimal VR cannot be achieved.

5 Conclusions

In this paper, the VR induced by the weak character signal with arbitrary high frequency is investigated in a fractional-order system. Through a scale transformation, we transform the high-frequency signal excited system to the low-frequency signal excited system. When the VR occurs in the rescaled system, it also occurs in the original system. The dynamics of the rescaled system and the original system are equivalent. The VR can be analyzed by both analytical methods and numerical simulations. The results by the two methods are in good agreement. The VR can occur in the overdamped and the underdamped fractional-order system with a bistable potential. If the system has a monostable potential, the VR is difficult to appear. The fractional order is a key factor in the response amplitude of the system. For larger values of the fractional order, the response amplitude usually has a larger value too. Another factor to influence the response amplitude is the reduction scale. The low frequency in the rescaled system mainly depends on the reduction scale, but is independent of the high frequency of the character signal. It indicates that the method can be used in the nonlinear system excited by an arbitrary high-frequency signal. It is a remarkable highlight of this paper. Our method in this paper provides a way to enhance the weak high-frequency signal. It can be used in the design of an electric equipment. By virtue of the method, we can determine the system parameters which can make the VR to appear at high frequency. Hence, it makes the application of the VR in detecting the weak character signal at arbitrary high frequency in the real world possible.

Acknowledgment

References

[1] Gammaitoni, L., Hänggi, P., Jung, P., and Marchesoni, F., 1998, "Stochastic Resonance," Rev. Mod. Phys., **70**(1), pp. 223–287.
[2] Liu, X., Yang, J., Liu, H., Cheng, G., Chen, X., and Xu, D., 2015, "Optimizing the Adaptive Stochastic Resonance and Its Application in Fault Diagnosis," Fluctuation Noise Lett., **14**(4), p. 1550038.
[3] Tan, J., Chen, X., Wang, J., Chen, H., Cao, H., Zi, Y., and He, Z., 2009, "Study of Frequency-Shifted and Re-Scaling Stochastic Resonance and Its Application to Fault Diagnosis," Mech. Syst. Signal Process., **23**(3), pp. 811–822.
[4] Landa, P. S., and McClintock, P. V. E., 2000, "Vibrational Resonance," J. Phys. A: Math. Gen., **33**(45), pp. L433–L438.
[5] Baltanás, J. P., Lopez, L., Blechman, I. I., Landa, P. S., Zaikin, A., Kurths, J., and Sanjuán, M. A. F., 2003, "Experimental Evidence, Numerics, and Theory of Vibrational Resonance in Bistable Systems," Phys. Rev. E, **67**(6), p. 066119.
[6] Chizhevsky, V. N., and Giacomelli, G., 2008, "Vibrational Resonance and the Detection of Aperiodic Binary Signals," Phys. Rev. E, **77**(5), p. 051126.
[7] Mbong, T. D., Siewe, M. S., and Tchawoua, C., 2015, "The Effect of Nonlinear Damping on Vibrational Resonance and Chaotic Behavior of a Beam Fixed at Its Two Ends and Prestressed," Commun. Nonlinear Sci. Numer. Simul., **22**(1–3), pp. 228–243.
[8] Shi, J., Huang, C., Dong, T., and Zhang, X., 2010, "High-Frequency and Low-Frequency Effects on Vibrational Resonance in a Synthetic Gene Network," Phys. Biol., **7**(3), p. 036006.
[9] Qin, Y. M., Wang, J., Men, C., Deng, B., and Wei, X. L., 2011, "Vibrational Resonance in Feedforward Network," Chaos, **21**(2), p. 023133.
[10] Yu, H., Wang, J., Sun, J., and Yu, H., 2012, "Effects of Hybrid Synapses on the Vibrational Resonance in Small-World Neuronal Networks," Chaos, **22**(3), p. 033105.
[11] Rajasekar, S., Used, J., Wagemakers, A., and Sanjuán, M. A. F., 2012, "Vibrational Resonance in Biological Nonlinear Maps," Commun. Nonlinear Sci. Numer. Simul., **17**(8), pp. 3435–3445.
[12] Hu, D., Yang, J., and Liu, X., 2012, "Delay-Induced Vibrational Multiresonance in FitzHugh–Nagumo System," Commun. Nonlinear Sci. Numer. Simul., **17**(2), pp. 1031–1035.
[13] Yang, L., Liu, W., Yi, M., Wang, C., Zhu, Q., Zhan, X., and Jia, Y., 2012, "Vibrational Resonance Induced by Transition of Phase-Locking Modes in Excitable Systems," Phys. Rev. E, **86**(1), p. 016209.
[14] Zhu, J., Kong, C., and Liu, X., 2016, "Subthreshold and Suprathreshold Vibrational Resonance in the FitzHugh–Nagumo Neuron Model," Phys. Rev. E, **94**(3), p. 032208.
[15] Abirami, K., Rajasekar, S., and Sanjuán, M. A. F., 2013, "Vibrational Resonance in the Morse Oscillator," Pramana, **81**(1), pp. 127–141.
[16] Yang, J. H., and Zhu, H., 2012, "Vibrational Resonance in Duffing Systems With Fractional-Order Damping," Chaos, **22**(1), p. 013112.
[17] Yang, J. H., Sanjuán, M. A. F., and Liu, H. G., 2015, "Bifurcation and Resonance in a Fractional Mathieu-Duffing Oscillator," Eur. Phys. J. B, **88**(11), p. 310.
[18] Yang, J. H., Sanjuán, M. A. F., Liu, H. G., and Cheng, G., 2015, "Bifurcation Transition and Nonlinear Response in a Fractional-Order System," ASME J. Comput. Nonlinear Dyn., **10**(6), p. 061017.
[19] Chen, L., Li, H., Li, Z., and Zhu, W., 2013, "Asymptotic Stability With Probability One of MDOF Nonlinear Oscillators With Fractional Derivative Damping," Sci. China: Phys. Mech. Astron., **56**(11), pp. 2200–2207.
[20] Monje, C. A., Chen, Y. Q., Vinagre, B. M., Xue, D., and Feliu, V., 2010, Fractional-Order Systems and Controls: Fundamentals and Applications, Springer-Verlag, London, pp. 10–12.
[21] Blekhman, I. I., and Landa, P. S., 2004, "Conjugate Resonances and Bifurcations in Nonlinear Systems Under Biharmonical Excitation," Int. J. Nonlinear Mech., **39**(3), pp. 421–426.
[22] Thomsen, J. J., 2003, Vibrations and Stability, Springer-Verlag, Berlin, pp. 287–334.
[23] Blekhman, I. I., 2000, Vibrational Mechanics, World Scientific, Singapore.
[24] Rajasekar, S., Jeyakumari, S., Chinnathambi, V., and Sanjuán, M. A. F., 2010, "Role of Depth and Location of Minima of a Double-Well Potential on Vibrational Resonance," J. Phys. A: Math. Theor., **43**(46), p. 465101.
[25] Rajasekar, S., Abirami, K., and Sanjuán, M. A. F., 2011, "Novel Vibrational Resonance in Multistable Systems," Chaos, **21**(3), p. 033106.
[26] Shen, Y., Yang, S., Xing, H., and Gao, G., 2012, "Primary Resonance of Duffing Oscillator With Fractional-Order Derivative," Commun. Nonlinear Sci. Numer. Simul., **17**(7), pp. 3092–3100.
[27] Shen, Y., Yang, S., Xing, H., and Ma, H., 2012, "Primary Resonance of Duffing Oscillator With Two Kinds of Fractional-Order Derivatives," Int. J. Nonlinear Mech., **47**(9), pp. 975–983.
[28] Van Khang, N., and Chien, T. Q., 2016, "Subharmonic Resonance of Duffing Oscillator With Fractional-Order Derivative," ASME J. Comput. Nonlinear Dyn., **11**(5), p. 051018.

[29] Yang, J. H., Sanjuán, M. A. F., Liu, H. G., Litak, G., and Li, X., 2016, "Stochastic P-Bifurcation and Stochastic Resonance in a Noisy Bistable Fractional-Order System," Commun. Nonlinear Sci. Numer. Simul., **41**, pp. 104–117.

[30] Balachandran, B., and Magrab, E. B., 2008, *Vibrations*, Cengage Learning, Toronto, ON, Canada, pp. 183–203.

[31] Magin, R., Ortigueira, M. D., Podlubny, I., and Trujillo, J., 2011, "On the Fractional Signals and Systems," Signal Process., **91**(3), pp. 350–371.

[32] He, Q., Wang, J., Liu, Y., Dai, D., and Kong, F., 2012, "Multiscale Noise Tuning of Stochastic Resonance for Enhanced Fault Diagnosis in Rotating Machines," Mech. Syst. Signal Process., **28**, pp. 443–457.

[33] Li, J., Chen, X., Du, Z., Fang, Z., and He, Z., 2013, "A New Noise-Controlled Second-Order Enhanced Stochastic Resonance Method With Its Application in Wind Turbine Drivetrain Fault Diagnosis," Renewable Energy, **60**, pp. 7–19.

[34] Wang, J., He, Q., and Kong, F., 2015, "Adaptive Multiscale Noise Tuning Stochastic Resonance for Health Diagnosis of Rolling Element Bearings," IEEE Trans. Instrum. Meas., **64**(2), pp. 564–577.

[35] Lang, R., Li, X., Gao, F., and Yang, L., 2016, "Re-Scaling and Adaptive Stochastic Resonance as a Tool for Weak GNSS Signal Acquisition," J. Syst. Eng. Electron., **27**(2), pp. 290–296.

[36] Yang, Y., Xu, W., Gu, X., and Sun, Y., 2015, "Stochastic Response of a Class of Self-Excited Systems With Caputo-Type Fractional Derivative Driven by Gaussian White Noise," Chaos Solitons Fract., **77**, pp. 190–204.

[37] Qin, Y., Tao, Y., He, Y., and Tang, B., 2014, "Adaptive Bistable Stochastic Resonance and Its Application in Mechanical Fault Feature Extraction," J. Sound Vib., **333**(26), pp. 7386–7400.

[38] Lu, S., He, Q., and Kong, F., 2015, "Effects of Underdamped Step-Varying Second-Order Stochastic Resonance for Weak Signal Detection," Digital Signal Process., **36**, pp. 93–103.